1.73 (3H, s, 8′), 1.67 (3H, s, 7′-Me), 1.32 (3H, s, 3′-Me); ^{13}C NMR (125 MHz, CD_3OD) δ 152.91 (C-3′), 147.62 (C-11), 147.39 (C-3), 146.69 (C-10), 146.63 (C-2), 133.27 (C-7′), 124.86 (C-6′), 122.72 (C-4a), 122.53 (C-12a), 122.05 (C-1a), 118.26 (C-8a), 116.26 (C-12), 116.15 (C-4), 114.17 (C-9), 113.46 (C-1), 111.41 (C-2′), 68.55 (C-13a), 61.61 (C-8), 58.27 (C-6), 46.69 (C-1′), 41.01 (C-4′), 29.83 (C-13), 27.04 (C-5′), 26.0 (C-8′), 24.38 (C-5), 17.91 (7′-Me), 16.79 (3′-Me); SIMS *m/z* $[M]^+$ 436; HRMS *m/z* $[M]^+$ 436.2487 ($C_{27}H_{34}NO_4$ requires 436.2482), *m/z* $[M\text{-}C_{10}H_{16}]^+$ 300.1241 ($C_{17}H_{18}NO_4$ requires 300.1235).

Antimicrobial assay. Antibacterial activities against *E. coli* (ATCC 25923) and *S. aureus* (ATCC 25922) were determined by means of the minimum inhibitory concentration (MIC) using the two-fold serial broth dilution test[7] in liquid nutrient medium and 24-well microplates. MIC was defined as the lowest concentration of the test substance which did not induce visible growth in comparison with a blank experiment. The substances were dissolved in DMSO (final concentration 2.5%). Dilutions with the test medium furnished concentrations from 3.9-250 μg/mL. Benzalkonium and benzethonium chloride were used as standards. The several 24-well plates in which each well contained an appropriate growth medium with a different concentration of the respective test samples were incubated with the test organism. The 24-well plate was incubated at 37°C for 24 h for bacteria. Bacteria tested were preliminarily cultivated in 3% nutrient broth ('Nissui', Japan) at 37°C. All experiments were run in duplicate or triplicate.

***In vitro* cytotoxicity assay (SRB assay).** Cytotoxicity was evaluated using a standard HTCL assay. The assay was carried out according to the standard SRB assay procedure described by Rubinstein *et al.*[10] Samples were tested first by prescreening against KB at 40, 4, and 0.4 μg/mL for a two-day exposure period. Active compounds that inhibited KB cell growth ≥ 40% relative to control at 4 μg/mL were re-tested in a dose-response study against an HTCL panel. Drug stock solutions were prepared in DMSO, and the final solvent concentration was 2% DMSO (v/v), a concentration without effect on cell replication. The human tumor cell line panel constituted of lung carcinoma (A-549), prostate carcinoma (DU-145), epidermoid carcinoma of the nasopharynx (KB), and KBvin (drug resistant), and human promyelocytic leukemia (HL-60). Cells were cultured at 37°C in RPMI-1640 with 100 μg/mL kanamycin and 10% (v/v) fetal bovine serum in a humidified atmosphere containing 5% CO_2. Initial seeding densities varied among the cell lines to ensure a final absorbance reading in control cultures in the range 1-2.5 A_{562} units. Drug exposure was for 3 days, and the ED_{50} value (μg/mL), the drug concentration that reduced the absorbance by 50%, was interpolated from dose-response data. Each test was performed in triplicate, and absorbance readings varied no more than 5%. ED_{50} values determined in independent tests varied no more than 30%.

***In vitro* cytotoxicity assay (MTT assay).** All cell lines were propagated in RPMI-1640 medium

supplemented with 10% (v/v) FBS, 100 U/mL penicillin and 100 μg/mL streptomycin at 37°C in a humidified atmosphere of 5% CO_2 and 95% air. Cell viability was measured by the MTT [3-(4,5-dimethythiazol-2-yl)-2,5-diphenyltetrazolium bromide] colorimetric method. Cells were seeded at densities of 5,000–10,000 cells/well in 96-well tissue culture plates. On day two, cells were treated with test compounds for another 72 h. After drug treatment, attached cells were incubated with MTT (0.5 mg/mL, 1 h) and subsequently solubilized in DMSO. The absorbancy at 550 nm was then measured using a microplate reader. The ED_{50} (μg/mL) is the concentration of agent that reduced cell viability by 50% under the experimental conditions.

***In vitro* cytotoxicity assay (WST-8 assay).** *Cell Cultures.* Human promyelocytic leukemia HL-60 cells were purchased from Dainippon Pharmaceutical Co., Ltd., and maintained in RPMI-1640 medium (Sigma), supplemented with 10% heat-inactivated fetal bovine serum (Sigma) and 2 mM L-glutamine (Sigma) at 37 °C in a humidified atmosphere containing 5% CO_2. The doubling time of cells was approximately 24 h. *WST-8 Assay.*[17] The test compounds were dissolved in DMSO at 50 mM and stored at -20°C. These stock solutions were further diluted with medium from 50 to 0.6 μM prior to use. The final concentrations of DMSO in the culture medium were less than 0.1%. 0.1% DMSO-treated cells were used as the control for all experiments. Cytotoxic effects of test compounds on HL-60 cells were detected by the WST-8 assay. HL-60 cells were plated at 5×10^3 cells/90 μL medium/well into 96-well plates. After overnight growth, cells were treated with various concentrations of test samples for 48 h. Following incubation with test compounds, cell viability was assayed with a Cell Counting Kit-8 (Dojindo Molecular Technologies). Ten microliters of WST-8 solution (5 mM) was added to each well and then incubated for 3 h. The relative viability of cells was determined by measuring the absorbance at 450 nm (reference at 650 nm) with a micro plate reader Anthos Lucy 2 (Aloka Co., Ltd.,). The IC_{50} (μg/mL) is the concentration of agent that reduced cell viability by 50% under the experimental conditions.

***In vitro* EBV-EA activation experiment.**[24] The inhibition of EBV-EA activation was assayed using Raji cells (virus non-producer) which were cultivated in 8% FBS RPMI 1640 medium. The indicator Raji cells (1×10^6 cells/ml) were incubated at 37 °C for 48 h in 1 ml of the medium containing *n*-butyric acid (4 mM, inducer), 32 pmol of TPA (20 ng/ml in DMSO), and 32, 16, 3.2, and 0.32 nmol of the test compound (DMSO solution). Smears were made from the cell suspension. The activated cells were stained by high-titer EBV-EA positive sera from nasopharyngeal carcinoma (NPC) patients and detected by a conventional indirect immunofluorescence technique. In each assay, at least 500 cells were counted, and the experiments were repeated three times. The average extent of EA induction was compared with that of positive control experiments with *n*-butyric acid (4 mM) plus TPA (32 pmol) in which EA

induction was ordinarily around 40%. In this screening method, the cell viability required for the judgment of inhibitory effects was more than 60%.

Determination of the scavenging effect on DPPH radicals.[25] Ethanol (100 μl) was added to individual wells of a 96-well plate. The test compounds were dissolved in DMSO and diluted with EtOH to adjust to 500 μM concentration. The final solvent concentration was 0.25% DMSO (v/v). The sample solution (100 μl) was added to individuals by the 2-fold dilution, and EtOH solution (100 μl) of DPPH radical (final concentration was 100 μM) was also added. The final concentration of the test compounds was from 0.24 to 250 μM. A control sample containing EtOH solution (100 μl) of DPPH radical and EtOH (100 μl) was prepared in the 96-well plate, which was incubated at 25 °C for 30 min in the dark. After incubation, the decrease in absorbance was determined by measuring the optical density change at 550 nm with a microplate luminescence reader Lucy 2 (ALOKA). The radical-scavenging activity expressed as % inhibition against DPPH radical, was calculated according to Yen and Duh (1994): % Inhibition = $[(A_B-A_A)/A_B]\times100$, (A_A is the absorbance of the tested sample after 30 min; A_B is the absorbance of the blank sample). The data presented are the average from two or three independent experiments.

***In vitro* antimalaria screening.** *Parasites.* In all of the studies described in this report, *P. falciparum* strain FCR-3(ATCC 30932) was used.[26, 27] Human serum and erythrocytes were obtained from healthy donors, stored at 4°C and used within 10-14 days from donation. Parasites were cultured in 10% heat inactivated A^+ human erythrocytes and suspended at a 5% hematocrit in RPMI 1640 medium (Gibco, NY) which contained 50 mg of gentamicin per liter, and 10% group A^+ human serum and was buffered with 25 mM *N*-2-hydroxyethylpiperazine-*N'*-2-ethansulfonic acid (HEPES, pH 7.4) and 25 mM $NaHCO_3$. Cultures were maintained at 37 °C in a gas mixture of 5% O_2-5% CO_2-90% nitrogen.[28] *Drug testing.* Various concentrations of compounds, suspended in 10 μl of distilled water, were added to individual wells of a 24-well plate. Erythrocytes with 0.3% parasitemia were added to each well in 990 μl of culture medium to give a final hematocrit of 3%. The plates were incubated at 37 °C for 72 h under 5% O_2-5% CO_2-90% nitrogen. Parasite morphology in drug-treated culture after 72 hrs was measured by staining with Giemsa, and the number of parasitized red blood cells per 10,000 erythrocytes was counted and growth rates were calculated. All compounds were run in duplicate at each concentration. Drug-free control cultures were run simultaneously. All data points represent means of at least two experimental tests. The 50% inhibitory concentration (EC_{50}) was defined by comparison with drug-free controls incubated under the same conditions.[29,30] *Mammalian cells.* A wild-type mouse FM3A cell line (subclone F-28-7) was supplied by the Health Sciences Research Resources Bank (Osaka, Japan).

FM3A cells were maintained in suspension culture at 37°C in a 5% CO_2 atmosphere in plastic bottles containing ES medium (Nissui Pharmaceutical Co., Ltd., Tokyo, Japan) supplemented with 2% heat-inactivated fetal bovine serum (Gibco, NY).[31,32] *Toxicity to mammalian cells.* The cell line grew with a doubling time of about 12 h. Before being exposed to drugs, cells were seeded at 990 μl of a density of 5×10^4 cells/ml, and various concentrations of compounds dispensed in 10 μl of distilled water were added to individual wells of a 24-well plate. The plates were incubated at 37 °C in a 5% CO_2 atmosphere for 48 hrs. Cell numbers were measured using a blood cell counter CC-108 (Toa Medical Electric Co., Japan). All data points represent means of at least two experimental tests. The 50% inhibitory concentration (IC_{50}) is defined by comparison with that of drug-free controls incubated under the same conditions. Cell growth inhibition is the index of cytotoxicity including cytostatic activity of the test compounds. *Selective toxicity.* Selective toxicity was estimated from the ratio (IC_{50}/EC_{50}) of the drug concentrations necessary to inhibit the growth rate of cells to 50% of the growth value between the malaria parasites and mouse mammary FM3A cells which served as a model host.[33]

Anti-HIV assay. The T cell line H9 was maintained in continuous culture with complete medium (RPMI 1640 with 10% fetal calf serum [FCS] supplemented with L-glutamine) at 5% CO_2 and 37 °C. Aliquots of this cell line were used in experiments only when in the log-phase of growth. Test samples were first dissolved in DMSO. The following are the final drug concentrations routinely used for screening: 100, 20, 4, and 0.8 μg/mL. For active agents, additional dilutions are prepared for subsequent testing so that accurate EC_{50} values (see definition below) could be achieved. As the test samples were being prepared, an aliquot of H9 cells was infected with HIV-1 (IIIB isolate), while another aliquot was mock-infected with complete medium. The mock-infected sample was used for toxicity determinations (IC_{50}, see definition below). The stock virus used for these studies typically had a $TCID_{50}$ value of 10^4 Infectious Units (IU)/mL. The appropriate amount of virus for a multiplicity of infection between 0.1 and 0.01 IU/cell was added to the first aliquot of cells. The other aliquot of cells received only culture medium and was then incubated under identical conditions to the HIV-infected cells. After 4 h incubation at 37 °C and 5% CO_2, both cell populations were washed three times with fresh medium and then added to the appropriate wells of a 24-well plate containing various concentrations of the test drug or culture medium (positive infected control/negative-control drug). In addition, AZT was also assayed during each experiment as a positive-control drug. The plates were incubated at 37 °C and 5% CO_2 for 4 days. Cell-free supernatants were collected on day 4 and tested by an in-house p24 antigen ELISA assay; p24 antigen is a core protein of HIV and, therefore, is an indirect measure of virus present in the supernatants. Toxicity was determined by performing cell counts by a coulter counter on the mock-infected cells, which had received either culture medium (no toxicity), test sample or AZT. If a

test sample had suppressive capability and was not toxic, its effects wre reported in the following terms: IC_{50}, the concentration of test sample that was toxic to 50% of the mock-infected cells; EC_{50}, the concentration of the test sample that was able to suppress HIV replication by 50%; and therapeutic index (TI), the ratio of IC_{50} to EC_{50}.

ACKNOWLEGEMENT

This work was supported in part by a grant from the National Cancer Institute Grant CA-17625 awarded to K. H. Lee.

REFERENCES.

1. F. Pojer, E. Wemakor, B. Kammerer, H. Chen, C. T. Walsh, S.-M. Li, and L. Heide, *Proc. Natl. Acad. Sci.*, 2003, USA 100, 2316.
2. D. J. Edwards and W. H. Gerwick, *J. Am. Chem. Soc.*, 2004, **126**, 11432.
3. T. Kuzuyama, J. P. Noel, and S. B. Richard, *Nature,* 2005, **435**, 983.
4. M. Tello, T. Kuzuyama, L. Heide, J. P. Noel, S. B. Richard, *Cell Mol. Life Sci.*, 2008, **65**, 1459.
5. S.-M. Li, *Phytochemistry*, 2009, **70**, 1746.
6. T. Usui, M. Kondoh, C. B. Cui, T. Mayumi, and H. Osada, *Biochem. J.*, 1998, **333**, 543.
7. B. Botta, A. Vitali, P. Menendez, D. Misiti, and M. G. Delle, *Curr. Med. Chem.*, 2005, **12**, 717.
8. K. Iwasa, M. Moriyasu, Y. Tachibana, H.-S Kim, Y. Wataya, W. Wiegrebe, K. F. Bastow, L. M. Cosentino, M. Kozuka, and K. H. Lee, *Bioorg. Med. Chem.*, 2001, **9**, 2871.
9. W. H. Cui, K. Iwasa, H. Tokuda, A. Kashihara, Y. Mitani, T. Hasegawa, Y. Nishiyama, M. Moriyasu, H. Nishino, M. Hanaoka, C. Mukai, and K. Takeda, *Phytochemistry*, 2006, **67**, 70.
10. L. V. Rubinstein, R. H. Shoemaker, K. D. Paull, R. M. Simo, R. S. Tosini, P. Skehan, P. A.Scudiero, A. Monks, and M. R. Boyd, *J. Natl. Cancer Inst.*, 1990, **82**, 1113.
11. Y. Ito, S. Yanase, J. Fujita, T. Harayama, T. Takashima, and H. Imanaka, *Cancer Lett.*, 1981, **13**, 29.
12. Y. Kashiwada, F. Hashimoto, L. M. Cosentino, C. H. Chen, P. E. Garrett, and K. H. Lee, *J. Med. Chem.*, 1996, **39**, 1016.
13. K. Iwasa, S. Okada, Y. Nishiyama, S. Takeuchi, M. Moriyasu, C. Tode, M. Sugiura, A. Takeuchi, H. Tokuda, K. Takeda, Y.-N. Liu, P-.C. Wu, K. F. Bastow, T. Akiyama, and K. H. Lee, *Heterocycles*, 2009, **77**, 1355.
14. B. Delley, *J. Chem. Phys.*, 1990, **92**, 508.
15. B. Delley, *J. Chem. Phys.*, 2000, **113**, 7756.
16. T. Mosmann, *J. Immunol. Methods*, 1983, **16**, 55.

17. M. Ishiyama, Y. Miyazono, K. Sasamoto, Y. Ohkura, and K. Ueno, *Taranta*, 1997, **44**, 1299.
18. A. Murakami, H. Ohigashi, and K. Koshimizu, *Biosci. Biotechnol. Biochem.*, 1996, **60**, 1.
19. K. Yasukawa, M. Takido, T. Matsumoto, M. Takeuchi, and S. Nakagawa, *Oncology*, 1991, **48**, 72.
20. T. Konoshima, M. Takasaki, M. Kozuka, T. Nagao, H. Okabe, N. Irino, T. Nakasumi, H. Tokuda, and H. Nishino, *Biol. Pharm. Bull.*, 1995, **18**, 284.
21. J. P. Perdew and Y. Wang, *Phys. Rev. B*, 1992, **45**, 13244.
22. A. D. Becke, *J. Chem. Phys.*, 1988, **88**, 2547.
23. C. Lee, W. Yang, and R. G. Parr, *Phys. Rev. B,* 1988, **37**, 786.
24. Y. Takemura, M. Ju-ichi, C. Ito, H. Furukawa, and H. Tokuda, *Planta Med.*, 1995, **61**, 366.
25. M. S. Blois, *Nature*, 1958, **181**, 1199.
26. W. Trager and J. B. Jensen, *Science,* 1976, **193**, 673.
27. J. B. Jensen, W. Trager, and J. Doherty, *Exp. Parasitol*, 1979, **48**, 36.
28. R. W. Winter, K. A. Cornell, L. L. Johnson, M. Ignatushchenko, D. J. Hinrivhs, and M. K. Riscoe, *Antimicrob Agents Chemother.*, 1996, **40**, 1408.
29. A. V. O. Ofulla, V. C. N. Okoye, B. Khan, J. I. Githure, C. R. Roberts, A. J. Johnson, and S. K. Martin, *Am. J. Trop. Med. Hyg.*, 1993, **49**, 335.
30. H. Asahi and T. Kanazawa, *Parasitology*, 1994, **109**, 397.
31. A. Yoshioka, S. Tanaka, O. Hiraoka, Y. Koyama, Y. Hirota, D. Ayusawa, T. Seno, C. Garrett, and Y. Wataya, *J. Biol. Chem.*, 1987, **262**, 8235.
32. Y. Wataya and O. Hiraoka, *Biochem. Biophys. Res. Commun,* 1984, **123**, 677.
33. I. S. Shin, H. Tanifuji, Y. Arata, Y. Morizawa, T. Nakayama, and Y. Wataya, *Parasitol. Res.*, 1995, **81**, 622.

the FEBS Journal

Association of RNase L with a Ras GTPase-activating-like protein IQGAP1 in mediating the apoptosis of a human cancer cell-line

Akira Sato[1], Tomoharu Naito[1], Akiko Hiramoto[1], Kazato Goda[1], Takuya Omi[1], Yukio Kitade[2], Takuma Sasaki[3], Akira Matsuda[4], Masakazu Fukushima[1], Yusuke Wataya[1] and Hye-Sook Kim[1]

1 Department of Molecular Drug Informatics, Faculty of Pharmaceutical Sciences, Okayama University, Japan
2 Department of Biomolecular Science, Faculty of Engineering, Gifu University, Japan
3 Department of Bioorganic Chemistry, School of Pharmacy, Aichi Gakuin University, Nagoya, Japan
4 Department of Medicinal Chemistry, Faculty of Pharmaceutical Sciences, Hokkaido University, Sapporo, Japan

Keywords
apoptosis; ECyd; focused proteomics; IQGAP1; RNase L

Correspondence
H.-S. Kim, Faculty of Pharmaceutical Sciences, Okayama University, Tsushima, Okayama 700-8530, Japan
Fax: +81 86 251 7974
Tel: +81 86 251 7975
E-mail: hskim @cc.okayama-u.ac.jp

Note
Akira Sato and Tomoharu Naito contributed equally to this work

(Received 14 April 2010, revised 28 July 2010, accepted 26 August 2010)

doi:10.1111/j.1742-4658.2010.07833.x

Mammalian intracellular ribonuclease L (RNase L) is a latent endoribonuclease that functions against viral infections as an apoptosis-inducing protein, and its activity requires intracellular 5′-end-triphosphorylated-2′,5′ oligoadenylates (2-5A) as an activator. Previously, we showed that RNase L can be activated in human cancer cell line HT1080 by an RNA polymerase I inhibitor, 1-(3-*C*-ethynyl-β-D-*ribo*-pentofuranosyl)cytosine (3′-ethynylcytidine; ECyd). In ECyd-treated cells, knockdown of the RNase L resulted in a marked decrease in c-jun N-terminal kinase (JNK) phosphorylation, thereby inhibiting apoptosis. We investigate RNase L binding partners by focused proteomic approach using immunoprecipitation with anti-RNase L IgG and mass spectrometry. We found that the IQ motif-containing Ras GTPase-activating-like protein 1 (IQGAP1) can associate with RNase L, and that phosphorylation occurs on the IQGAP1. ECyd-induced JNK phosphorylation and apoptosis were inhibited when IQGAP1 was knocked down with a small interfering RNA. These results raise the interesting possibility that the RNase L–IQGAP1 association may regulate JNK phosphorylation in RNase L-madiated apoptosis. It is likely IQGAP1 works as a regulator in apoptosis.

Structured digital abstract

- MINT-7990574: *RNaseL* (uniprotkb:Q05823) *physically interacts* (MI:0914) with *Kinesin-like protein KIF23* (uniprotkb:Q02241) and *Ras GTPase-activating-like protein IQGAP1* (uniprotkb:P46940) by *anti bait coimmunoprecipitation* (MI:0006)
- MINT-7990598: *RNaseL* (uniprotkb:Q05823) *physically interacts* (MI:0915) with *IQGAP1* (uniprotkb:P46940) by *anti bait coimmunoprecipitation* (MI:0006)

Introduction

A cellular RNA-hydrolysing enzyme RNase L has an intriguing function in inducing cell death. This mammalian protein is a latent endonuclease that can work against viral infections by inducing apoptotic death of the infected cell [1,2]. This particular role of the nuclease is a current focus of attention for many

Abbreviations
2-5A, 5′-end-triphosphorylated-2′,5′ oligoadenylates; ECyd, 1-(3-*C*-ethynyl-β-D-*ribo*-pentofuranosyl)cytosine (3′-ethynylcytidine); IQGAP1, IQ motif-containing Ras GTPase-activating-like protein 1; JNK, c-jun N-terminal kinase; siRNA, small interfering RNA.

laboratories [3–9]. In order to initiate the apoptosis, RNase L has to be activated by intracellular 5′-end-triphosphorylated-2′,5′-oligoadenylates (2-5A). In this activation, 2-5A binds to RNase L at its N-terminal ankyrin repeat domain, the 2-5A–RNase L complex then causes damage to the mitochondrial membrane, eventually leading to apoptotic cell death. Elucidation of the details in this intracellular event is important, for this 2-5A-RNase L pathway is implicated in responses to not only viral infections, but also several types of external stimuli [1,3–9]. We are particularly interested in the possibility of clarifying a case of an anticancer drug action in terms of the 2-5A-RNase L pathway. An RNA synthesis inhibitor, 1-(3-*C*-ethynyl-β-D-*ribo*-pentofuranosyl)cytosine (3′-ethynylcytidine; ECyd), has been shown to exhibit cancer cell-selective toxicity by causing apoptotic cell death [10–12]. Our recent work has shown that activated RNase L is involved in this process and that the events ensuing the RNase L activation are c-jun N-terminal kinase (JNK) activation, followed by mitochondrial membrane damage, leading to cell apoptosis [13].

We have attempted to find specific cellular proteins that have affinities to RNase L with a view to elucidating the mechanism of the apoptotic process. We performed this investigation using focused proteomic means, i.e. coimmunoprecipitation with an anti-RNase L IgG, coupled with analysis by nano-LC MS/MS to identify the coprecipitated proteins. Here, we describe the identification of IQ motif-containing Ras GTPase-activating-like protein 1 (IQGAP1), which bears a strong affinity to RNase L. Furthermore, we found that the IQGAP1–RNase L complex has newly incorporated phosphate group(s) on the IQGAP1.

Participation of IQGAP1 in this apoptotic cell death was verified using small interfering (si)RNA knockdown experiments. Administration of an siRNA targeting the RNase L gene effectively prevented apoptosis, and administration of siRNA against IQGAP1 had the same effect. Based on these results, we now propose a process in which the partnership between RNase L and IQGAP1 operates for apoptosis.

Results and Discussion

Identification of RNase L binding protein

We recently reported that siRNA-mediated knockdown of RNase L markedly decreased the phosphorylation of JNK and inhibited apoptosis in ECyd-treated HT1080 cells [13]. This suggested that RNase L might possess a phosphorylating function. It is known that the RNase L molecule has a kinase homology domain [1,2], the function of which remains unknown. It is possible, therefore, that the JNK might be bound to and then phosphorylated by RNase L. This supposition led us to investigate whether JNK might be bound to an RNase L that has been fixed on an antibody against RNase L. Thus, we performed immunoprecipitation of ECyd-treated HT1080 cell lysate by adding an anti-RNase L IgG. As a control, we used a lysate from cells not treated with ECyd. The precipitates were solubilized and analysed by SDS gel electrophoresis. The results are shown in Fig. 1 (with Fig. S1). We cut out 15 protein bands as having different intensities between the anti-RNase L IgG immunoprecipitants (RNase L binding proteins; Fig. 1, lane 2 and/or lane 4) and the Protein G agarose precipitation for nonspecific binders (Protein G agarose beads binding proteins; Fig. 1, lane 1 and/or lane 3). The marked bands (no. 1–8 and 2′-8′) were those that had been strongly bound to RNase L (Fig. 1, lanes 2 and 4). In the proteomic analysis using nano LC-MS/MS, no JNK was detected among the binders. Instead, six proteins (i.e. myosin-9, IQGAP1, myosin-IE, immunoglobulin protein and kinesin-like protein KIF23, in addition to RNase L) were identified in these 15 bands. We also obtained complementary data for the identification of the focused protein bands based on MS/MS experiments (Table 1). Myosin-9 was present in the band 1 and also in the Protein G precipitations lane (nonspecific binding protein). Myosin-i.e and its isoform were present in bands 3–6 and 3′–6′. The myosin-IE might have been directly recognized by anti-RNase L IgG (Fig. 2B, pointed by an asterisk). Thus, we consider that the myosin-9 and myosin-IE were non-specifically bound to Protein G agarose beads. In this experiment, RNase L was identified in bands 8 and 8′. Therefore, we thought that IQGAP1 may be a specific RNase L binding partner, as found in bands 2 and 2′.

IQGAP1 is a 190 kDa molecular scaffold containing several domains that are required to interact with numerous proteins [14–16]. These motifs include a calponin homology domain (calcium-binding domain of calponin), four IQ (Ile–Gln) motifs and a Ras GTPase-related domain. Known targets for IQGAP1 include calmodulin, Cdc42, Rac1, actin, β-catenin, E-cadherin, S100B, CLIP-170, MEK1/2 and ERK1/2. Through interactions with these proteins, IQGAP1 participates in multiple cellular activities, including transcription, cell–cell adhesion and regulation of the cytoskeleton [14–16]. In addition, Li *et al.* [17] reported that IQGAP1 is highly phosphorylated in human cells and that IQGAP1 is a target for protein kinase C.

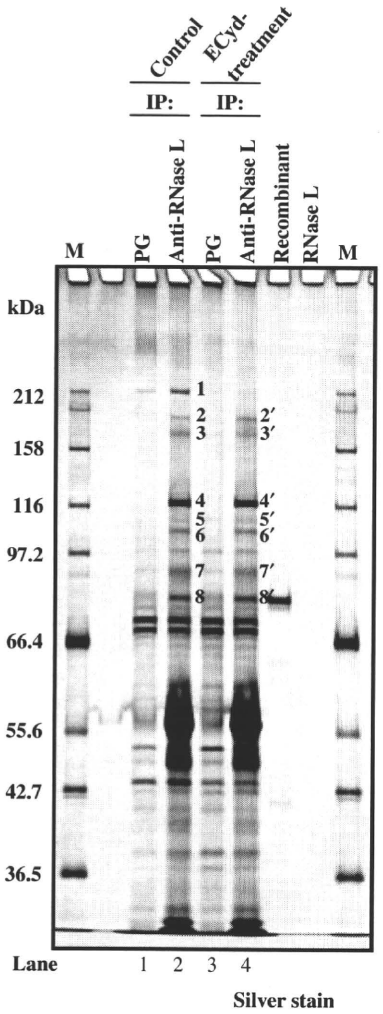

Fig. 1. Identification of RNase L binding proteins. Immunoprecipitation (IP) was done for RNase L from HT1080 cell extracts that had been treated with or without ECyd 1.3 μM for 24 h. Samples were loaded on 7.5% (w/v) SDS/PAGE and analysed by silver staining. The proteins analysed (bands 1–8 and 2′–8′) were excised from the silver-stained gel and digested in gel with trypsin. Extracted peptides were analysed by nano LC-MS/MS. PG; IP with Protein G only. Anti-RNase L; IP with anti-RNase L IgG. M; Protein size marker. All identified proteins are presented in Table 1.

To compare the RNase L–IQGAP1 association between ECyd-treated and -untreated cells, western blotting was performed with anti-IQGAP1 and anti-RNase L IgG individually. The intensities of both total IQGAP1 and total RNase L protein bands were not different between ECyd-treated and -untreated cells (Fig. 2A). It is notable, however, that the level of the IQGAP1 associated with RNase L was increased significantly in ECyd-treated cells (Fig. 2B). We measured the ratio of IQGAP1 associated with RNase L to total IQGAP1, and the results showed that 12% and 5% of total IQGAP1 was associated with RNase L in ECyd-treated cells and untreated cells, respectively (Fig. 2A,B).

To validate the interaction between RNase L and IQGAP1, we analysed the effect of RNase L knockdown on the association with these proteins. In the transfection with the RNase L-siRNA, the protein-band intensity of RNase L was decreased both in the cell lysate (A6) and in the immunoprecipitates (B6). The IQGAP1 in the immunoprecipitates was increased in ECyd-treated cells (B1, B2). The intensity of the IQGAP1 protein band in the immunoprecipitates of ECyd-treated RNase L knocked-down cells became the same as that in the untreated stage (B1, B2, B3). Interestingly, the IQGAP1 protein band in the whole-cell lysate was not different between the Ecyd treatment (A2) and RNase L knockdown (A3). siRNA with a four-base mismatch sequence (mismatch-siRNA; nonsilencing siRNA) had no effect on the interaction or the protein level (data not shown). These findings suggest that the association of RNase L and IQGAP1 was enhanced by ECyd treatment.

Phosphorylation of IQGAP1 after treatment with ECyd

We investigated the phosphorylation levels of endogenous IQGAP1 in ECyd-treated cells by using [^{32}P]-orthophosphate uptake experiments. Proteins were extracted from the cells and immunoprecipitated with anti-RNase-L IgG. From the resulting precipitate, proteins were eluted and resolved by PAGE. After transferring onto poly(vinylidene difluoride) membranes, the proteins were visualized by means of autoradiography. For comparison, whole-cell lysate without immunoprecipitation was submitted to the same analysis. The ^{32}P-labelled protein band was found in the position of IQGAP1 from ECyd-treated whole-cell lysates (Fig. 3A). The ^{32}P-labelled protein band was not detected in cells without ECyd treatment (Fig. 3A). However, immunoprecipitate experiments demonstrated that IQGAP1 associated with activated RNase L was labelled and the labelling with [^{32}P]-orthophosphate was high (fivefold higher: control, 15.70 ± 0.01; ECyd, 84.50 ± 3.82) in ECyd-treated cells but not in untreated cells (Fig. 3B).

Next, we investigated the mechanisms of IQGAPI phosphorylation regulated by RNase L in ECyd-treated cells. High levels in expression of IQGAP1 and RNase L were observed for cells in the untreated, in 2-5A-treated or ECyd-treated stages (Fig. 4A, lanes 1–3). However, the protein levels of phosphorylated

Table 1. Identification of RNase L binding protein.

Band no.	Identified protein	Accession no.[a]	Distinct peptides[b]	Score[c]	Sequence coverage	Theoretical M_r	Theoretical pI
1	Myosin-9	P35579	90	1452.88	49	226402.2	5.5
2	Ras GTPase-activating-like protein IQGAP1	P46940	35	434.16	25	189252.9	6.08
3	Myosin-IE	Q12965	15	184.38	17	127041.6	9.01
4	Myosin-IE	Q12965	48	714.46	44	127041.6	9.01
5	Myosin-IE	Q12965	10	132.27	11	127041.6	9.01
6	Myosin-IE	Q12965	12	165.84	15	127041.6	9.01
	Kinesin-like protein KIF23	Q02241	15	198.87	22	98106	8.69
7	Not identified[d]	–	–	–	–	–	–
8	2-5A-dependent ribonuclease (RNaseL)	Q05823	18	204.41	22	83533.2	6.2
2′	Ras GTPase-activating-like protein IQGAP1	P46940	27	357.81	20	189252.9	6.08
3′	Myosin-IE	Q12965	17	231.56	19	127041.6	9.01
4′	Myosin-IE	Q12965	42	640.24	41	127041.6	9.01
5′	Myosin-IE	Q12965	6	78.28	7	127041.6	9.01
6′	Myosin-IE	Q12965	12	189.97	17	127041.6	9.01
	Kinesin-like protein KIF23	Q02241	7	118.22	11	98106	8.69
7′	Not identified	–	–	–	–	–	–
8′	2-5A-dependent ribonuclease (RNaseL)	Q05823	26	353.11	33	83533.2	6.2

[a] Accession number from Swiss-prot protein database. [b] Number of matched peptides that in the an *in silico* the protein sequence. [c] Mill MS proteomic workbench prpbability-based peptide score calculated for MS/MS results. [d] No specific proteins were identifiable in MS/MS experiments.

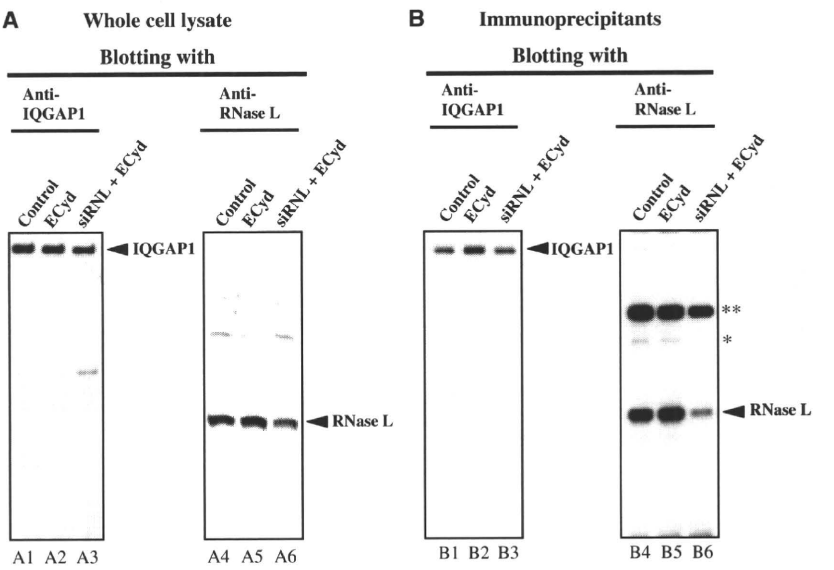

Fig. 2. Association of RNase L and IQGAP1. (A) Western blotting of whole-cell lysate. (B) Western blotting of immunoprecipitants. HT1080 cells (1.2×10^5) were transfected with RNase L-siRNA 5 nM in the presence of Lipofectamine 2000 2 $\mu g \cdot mL^{-1}$ for 24 h according to the manufacturer's protocol (Invitrogen), and then treated with ECyd 1.3 μM for 32 h. After ECyd treatment, cell lysates were immunoprecipitated with anti-RNase L IgG (B). Western blotting (WB) was probed with anti-RNase L and anti-IQGAP1 IgG, individually. The asterisks indicated nonspecific coimmunoprecipitated bands that cross-reacted with anti-RNase L IgG. Data are representative of at least three independent experiments. Control; Lipofectamine-only treatment, ECyd; ECyd treatment, siRNL+ECyd; RNase L-siRNA + ECyd treatment.

IQGAP1 in the immunoprecipitates were significantly higher both in 2-5A-treated and ECyd-treated cells in comparison with the control (Fig. 4A, lanes 4–6). In addition, the knockdown of RNase L markedly decreased total and phosphorylated IQGAP1 protein levels in the immunoprecipitates (Fig. 4B, lanes 3, 7).

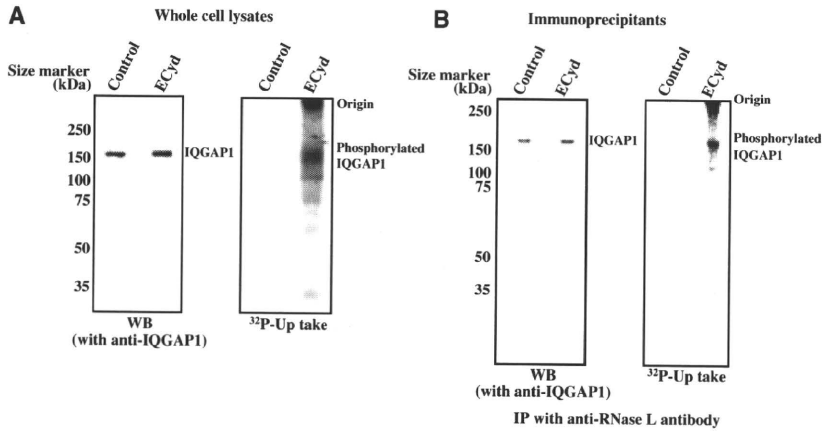

Fig. 3. Phosphorylation of IQGAP1 in ECyd-treated cells. HT1080 cells were incubated with [^{32}P]-orthophosphate in the presence of ECyd. Cells were solubilized and immunoprecipited with anti-RNase L IgG. (A) Analysis of whole-cell lysates: (left) western blotting with anti-IQGAP1 IgG, (right) ^{32}P-radioactivity. (B) Analysis of immunoprecipitants: (left) western blotting with anti-IQGAP1 IgG, (right) ^{32}P-radioactivity. The data represent three independent experiments.

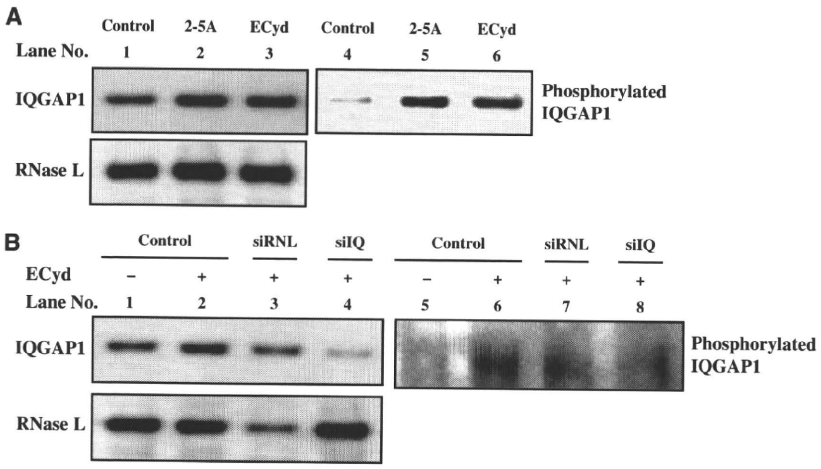

Fig. 4. Participation of RNase L in phosphorylating IQGAP1. (A) HT1080 cells were transfected with 2-5A(pApApA) 1 μM for 6 h (lanes 2, 5) and treated with ECyd 1.3 μM for 24 h (lanes 3, 6). Cell lysates were immunoprecipitated with anti-RNase L IgG, the precipitate was solubilized and the solution was submitted to gel electrophoresis. Western blotting was carried out with anti-IQGAP1 (upper left), anti-RNase L (lower left), and anti-phosphoserine/threonine/tyrosine sera (upper right). (B) HT1080 cells were transfected with siRNL; RNase L-siRNA 5 nM (lanes 3, 7) or siIQ; IQGAP1-siRNA 10 nM (lanes 4, 8) in the presence of Lipofectamine 2000 2 μg·mL^{-1} for 24 h, prior to ECyd 1.3 μM treatment. Cell lysates were immunoprecipitated with anti-RNase L IgG, the precipitate was solubilized and the solution was submitted to gel electrophoresis. Western blotting was carried out with anti-IQGAP1 (upper left) anti-RNase L (lower left), and anti-phosphoserine/threonine/tyrosine sera (upper right). The data represent three independent experiments.

Transfection of IQGAP1 siRNA led to decreases in both total IQGAP1 and phosphorylated IQGAP1 without affecting RNase L expression (Fig. 4B, lanes 4, 8).

In total, these results indicate that ECyd treatment can result in a distinctive increase in the proportion of phosphorylated IQGAP1 in the RNase L–IQGAP1 complex.

Prevention of ECyd-induced JNK phosphorylation and apoptosis by knocking down IQGAP1

The possibility that IQGAP1 functions to transmit apoptosis signals from RNase L to the JNK pathway was investigated. First, we explored the effect of IQGAP1 knockdown in ECyd-induced apoptosis. With ECyd-treated cells, expression of IQGAP1 was suppressed on administration of IQGAP1 siRNA and the number of apoptotic cells decreased, as measured by the TUNEL assay. Thus, we observed that the knockdown efficacy for IQGAP1 protein was > 60% by IQGAP1 siRNA transfection compared with that by mismatch-siRNA transfection (Figs 5A and S2). The number of ECyd-induced apoptotic cells was drastically decreased when IQGAP1 was knocked-down. By contrast, mismatch-siRNA transfection had no effect on ECyd-induced apoptosis (Fig. 5B,C). Next, in order to analyse the effect of IQGAP1 on

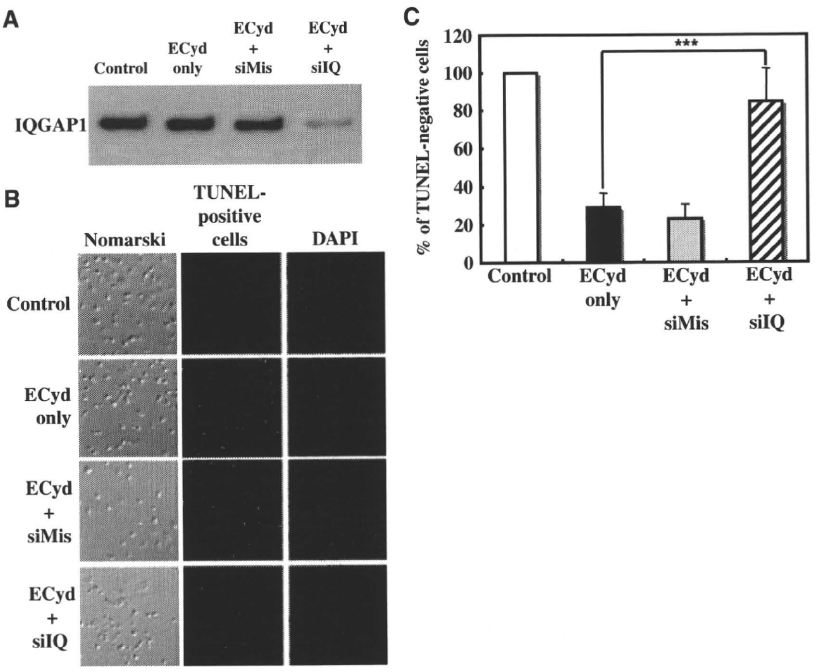

Fig. 5. Suppression of apoptosis in ECyd-treated cells with siRNA against IQGAP1. (A) HT1080 cells were transfected with siIQ; IQGAP1-siRNA 10 nM and siMis; mismatch-siRNA 10 nM in the presence of Lipofectamine 2000 2 $\mu g \cdot mL^{-1}$ for 24 h, and then treated with ECyd 1.3 μM for 32 h followed by western blot analysis. (B) Detection of apoptotic cells using the TUNEL assay. Apoptotic cells are shown in the green panel. Nuclei were stained with 4′,6-diamidino-2-phenylindole dihydrochloride. (C) Bar graph shows the percentage of TUNEL-negative cells in ECyd-treated HT1080 cells with or without siIQ transfection. $***P < 0.05$ total number of cells was counted at least 300 cells. Control, Lipofectamine 2000 treated cells.

the phosphorylation of JNK in HT1080 cells, siRNA for IQGAP1 was used to knockdown the IQGAP1 protein expression. The level of phosphorylated JNK was decreased in knocked-down cells, whereas the JNK-phosphorylation remained high in both the ECyd-only and ECyd-plus-mismatch-siRNA treatments. However, the fluorescence levels that represented the total JNK were the same in all of these treatments (Fig. 6). These findings indicate that IQGAP1 contributes to ECyd-induced JNK phosphorylation and apoptosis. Therefore, we consider that the association with RNase L and IQGAP1 plays a critical role in the apoptotic signaling pathway. Li *et al.* [9] suggested that JNK is an essential molecule in the apoptosis mediated by RNase L. Our recent work demonstrated that the knockdown of the RNase L in the ECyd-treated HT1080 cells dramatically decreased the phosphorylation of JNK, thereby inhibiting mitochondria-mediated apoptosis [13]. Therefore, the complex of IQGAP1 and RNase L may be regulating JNK phosphorylation in the RNase L-mediated apoptosis. Given the report of the IQGAP1 phosphorylation by protein kinase C [17], we think it possible that the observed IQGAP1 phosphorylation in the apoptosis may be mediated by either protein kinase C or/and by other proteins (e.g. RNase L). We are currently investigating the kinase activity of RNase L using *in vitro* assays (details to be published elsewhere). It is important to further investigate the mechanisms involved in this 'RNase L controlled IQGAP1 JNK phosphorylation' in apoptosis.

Conclusions

We have demonstrated that RNase L interacts with a partner, IQGAP1, and that this interaction is involved in promoting ECyd-induced apoptosis. In addition, we have shown that in this process IQGAP1 phosphorylation is enhanced. As the scheme in Fig. 7 indicates, we consider that the ECyd-induced apoptotic signal pathway is mediated by an RNase L–IQGAP1 association.

Materials and methods

Materials

ECyd was synthesized as described previously [10]. Lipofectamine 2000 was purchased from Invitrogen (Carlsbad, CA, USA). Human recombinant RNase L was prepared as described by Yoshimura *et al.* [18] and 2-5A was synthesized according to Lesiak and Torrence [19]. The IQGAP1 and phosphoserine/threonine/tyrosine antibodies were from Upstate Biotechnology (Lake Placid, NY, USA) and Abcam (Cambridge, UK), respectively. Preparation of mAb to human RNase L and synthesis of siRNA were performed as reported previously [20]. The siRNA against RNase L (RNase L-siRNA) and the control siRNA with four-base mismatch (mismatch-siRNA) used were as follows: RNase L-siRNA, 5′-GCUGUUCAAAACGAAGAUGTT-3′ 3′-TTCGACAAGUUUUGCUUCUAC-5′; mismatch-siRNA, 5′-GCUAUUCUAAAGGAAUAUGTT-3′ 3′-TTCGAUAAGAUUUCCUUAUAC-5′. The TT dinucleotide attached to

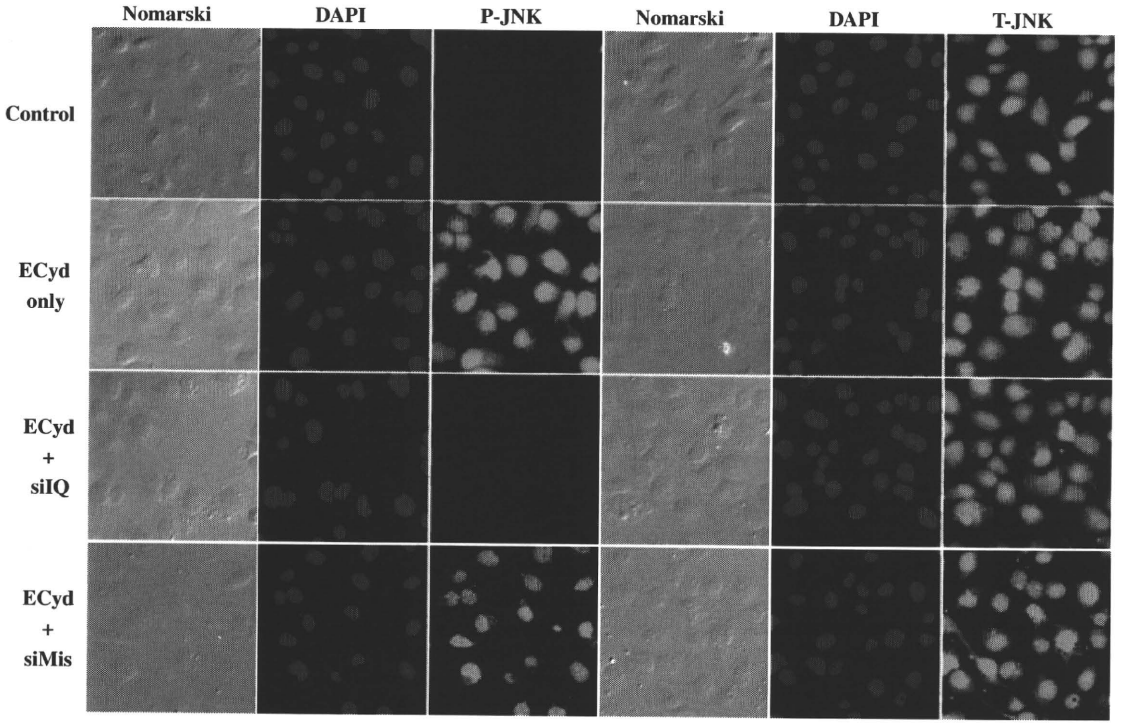

Fig. 6. Inhibition of JNK phosphorylation in ECyd-treated cells with siRNA against IQGAP1. HT1080 cells were transfected with siIQ; IQGAP1-siRNA 10 nM and siMis; mismatch-siRNA 10 nM in the presence of Lipofectamine 2000 2 $\mu g \cdot mL^{-1}$ for 24 h, and then treated with ECyd 1.3 μM for 24 h followed by immunofluorescence staining. Phosphorylated JNK (P-JNK) and total JNK (T-JNK) were detected by immunofluorescence with specific antiboby (Cell Signaling Technology). Nuclei were stained with 4′,6-diamidino-2-phenylindole dihydrochloride. Green fluorescence represents IF: P-JNK and T-JNK. Control indicates lipofectamine-only treated cells. The set of data in a given column were obtained from image-photos taken with a fixed exposure time.

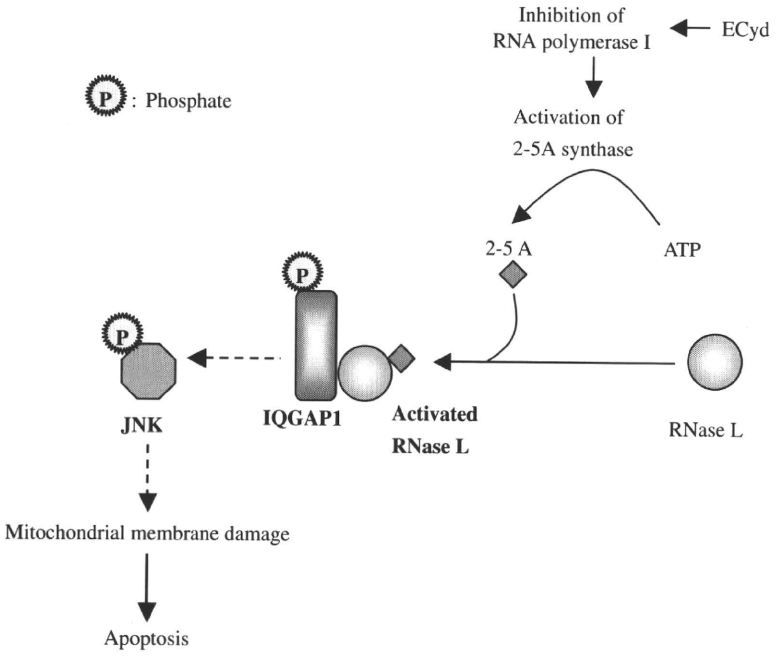

Fig. 7. Scheme of apoptotic signal pathway mediated by RNase L–IQGAP1 association in ECyd-treated cells. ECyd, an RNA polymerase I inhibitor, has potent cytotoxic activity against human cancer cells. In ECyd-treated cells, RNase L is activated and involved in JNK phosphorylation, which then induces mitochondria-dependent apoptosis. In the cell-death mechanisms, we hypothesize that RNase L mediates the phosphorylation of IQGAP1, the phosphate is then transferred to JNK, and the JNK-phosphorylation triggers apoptosis.

each of these oligonucleotides at their 3′-overhang was a 2′-deoxythymidine dimer with a carbamate linkage. It is known that carbamate internucleoside linkages enhance the siRNA silencing activities [20]. The IQGAP1-siRNA (Hs_IQGAP1_5_HP Validated siRNA, Catalog number SI02655268) and Nonsilencing-siRNA (AllStars Negative Control siRNA, Catalog number 1027280) were purchased from Qiagen (Hilden, Germany). ^{32}P-Orthophosphate, carrier-free, was from Perkin–Elmer (Waltham, MA, USA).

Cell culture and transfection for gene silencing

The human fibrosarcoma HT1080 cell line (American Type Culture Collection, Rockville, MD, USA) was cultured as described previously [11,12]. Transfection of siRNAs into HT1080 cells for silencing genes was performed as described previously, by administration with Lipofectamine 2000 [13,20,21].

Immunoprecipitation

HT1080 cells were gently lysed with RIPA buffer (50 mM Tris/HCl, pH 8.0, with 150 mM sodium chloride, 1.0% NP-40, 0.5% sodium deoxycholate and 0.1% SDS; Product number R0278; Sigma-Aldrich, St. Louis, MO, USA) with protease and phosphatase inhibitors (Sigma-Aldrich) for 30 min on ice and then centrifuged at 15 000 ***g*** at 4 °C for 15 min. The supernatant collected as cell lysate ($\sim 3 \times 10^6$ cells equivalent) was treated with 30 μL Protein G–Sepharose beads (ImmunoPure Immobilized Protein-G plus; Pierce, Rockford, IL, USA) to remove nonspecific binding proteins, and then incubated with 5 μg of anti-RNase L IgG at 4 °C for 4 h. The lysate was then incubated with an additional 30 μL of Protein G agarose beads at 4 °C for 12 h. The immunoprecipitated complexes were washed three times with RIPA buffer supplemented with protease and phosphatase inhibitors (Sigma-Aldrich). RNase L–protein complexes were eluted from the beads by heating at 95 °C for 5 min in 1 × SDS/sample buffer (62.5 mM Tris/HCl, pH 6.8, 25% glycerol, 2% SDS, 0.01% Bromophenol Blue; #161-0737; Bio-Rad, Hercules, CA, USA) supplemented with 5% β-mercaptoethanol and used for western blot analysis. This immunoprecipitation procedure was based on *Current Protocols in Molecular Biology* [22].

Western blotting

HT1080 cells were suspended in 20 mM Hepes (pH 7.5), 10 mM potassium acetate, 15 mM magnesium acetate, 1 mM dithiothreitol, 1 mM phenylmethanesulfonylfluoride, 10 μg·mL^{-1} aprotinin and 0.5% (v/v) Nonidet P-40, and homogenized by Dounce homogenizer on ice. Insoluble materials were removed by centrifugation at 10 000 ***g***, at 4 °C for 10 min. Proteins in soluble fractions were separated on 7.5% polyacrylamide SDS/gels, and transferred to poly(vinylidene difluoride) membranes (Millipore, Bedford, MA, USA). For detection of IQGAP1, HT1080 cells were gently lysed with RIPA buffer supplemented with protease and phosphatase inhibitors for 30 min on ice, and then the mixture was centrifuged at 15 000 ***g*** at 4 °C for 15 min. The supernatant was diluted with an equal amount of 2 × SDS sample buffer supplemented with 10% β-mercaptoethanol. This sample was boiled for 5 min, and proteins (20 μg) were separated by 12.5% PAGE. Western blotting was carried out with individual antibodies. The secondary antibody used was horseradish peroxidase-conjugated anti-mouse IgG (GE Healthcare, Little Chalfont, Buckinghamshire, UK). The protein bands were visualized using an ECL-plus western blotting detection system (GE Healthcare). Protein expression was quantified using VersaDoc imaging system (Bio-Rad).

HPLC-Chip-MS/MS

Tryptic digestion of proteins and MS analysis were carried out as described previously [23]. HPLC-Chip-MS/MS experiments were performed using an Agilent 1100 LC/MSD-Trap-XCT series system. The ionization system was the Chip Cube using HPLC-Chip-MS. The chip was automatically loaded and positioned into the MS nanospray chamber. The chip contained a Zorbax 300SB-C_{18} (40 nL, 5 μm) enrichment column and a Zorbax 300SB-C_{18} (43 mm × 75 μm, 5 μm) analysis column. The sample loading into the enrichment column was performed at a flow rate of 4 μL·min^{-1} with a 0.1% HCOOH in H_2O. LC gradient (mobile phase A: 0.1% HCOOH in H_2O; mobile phase B: 0.1% HCOOH and 10% H_2O in CH_3CN) was delivered at a flow rate of 300 nL·min^{-1}. Tryptic peptides were eluted from the reversed-phase column into the mass spectrometer using a linear gradient elution of 4–85% phase B over 40 min. The capillary voltage was set to 1850 V, the flow at 4 L·min^{-1}, and the temperature of the drying gas at 300 °C.

Database searches were performed against the Swiss-Prot database (release 51.3 of 12 December 2006) using a spectrum Mill MS proteomic workbench offered by Agilent (software version; A. 03. 020. 060). The search parameters were set so that they allowed the peptide mass tolerance at ± 2.5 Da and the fragment ion tolerance at ± 0.7 Da. The allowance also included matching peptides containing one miscleavage, selection of species (*Homo sapiens*), fixed modification of carbamidomethylated cysteines, and a variable modification of methionine oxidation. Identification of proteins was validated when at least two peptide sequences matched with the database sequences, with concomitant occurrence of the peptide score > 11.

Radiolabelling and protein fractionation

HT1080 cells were rinsed twice with phosphate-free RPMI 1640 medium containing BSA (which had been dial-

ysed overnight against phosphate-free RPMI 1640). The cells were incubated with ECyd in the phosphate-free RPMI 1640 at 37 °C for 14 h, and then with 1 $mCi \cdot mL^{-1}$ ^{32}P-orthophosphate (^{32}P-Pi) at 37 °C for 2 h. Cells were rinsed twice with NaCl/P_i and then lysed with RIPA buffer. The cell lysate was centrifuged at 15 000 *g* at 4 °C for 10 min, and the supernatant was collected for immunoprecipitation with anti-RNase L IgG (see below). Immunoprecipitated samples were submitted to SDS/PAGE (7.5% acrylamide gel). The gels were then wrapped in thin plastic films and exposed to a phospho-imager screen for recording their radioactivities. The recorded imaging plates were scanned with BAS1800II (FUJIFILM, Tokyo, Japan).

TUNEL assays for cell viability

The assays were carried out according to the TdT-mediated dUTP-biotin Nick End Labeling (TUNEL) protocol (#TB235; Promega, Madison, WI, USA) as described previously [13].

Immunofluorescence

After ECyd treatment, HT1080 cells were placed on coverglass plates. The cells were washed three times with NaCl/P_i and fixed with 3% formaldehyde in NaCl/P_i for 10 min. After fixation, cells were washed twice with NaCl/P_i, and were made permeable by treatment with 0.2% Triton X-100 in cold NaCl/P_i for 5 min. The slides were then incubated with NaCl/P_i containing 0.5% BSA as a blocking agent against nonspecific surface adsorption of antibodies for 30 min prior to treatment for 1 h with 1 $\mu g \cdot mL^{-1}$ anti-phosphorylated-JNK or anti-total-JNK serum (Cell Signaling Technology, Beverly, MA, USA). The cells were then incubated with 5 $\mu g \cdot mL^{-1}$ fluorescein-labelled goat anti-mouse IgG and 1 $\mu g \cdot mL^{-1}$ 4′,6-diamidino-2-phenylindole dihydrochloride for 30 min. Cells were washed three times with NaCl/P_i and covered with PermaFluor aqueous mounting medium (Invitrogen, Eugene, OR, USA). Stained cells were observed with an Olympus BX60 microscope (Olympus, Tokyo, Japan) fitted with appropriate fluorescence filters.

Acknowledgements

The authors thank Dr Hikoya Hayatsu (Faculty of Pharmaceutical Sciences, Okayama University) for helpful discussions. This research was partially supported by the Ministry of Education, Culture, Sports, Science and Technology for Exploratory Research (18659029, YW).

References

1 Bisbal C & Silverman RH (2007) Diverse functions of RNase L and implications in pathology. *Biochimie* **89**, 789–798.

2 Townsend HL, Jha BK, Han JQ, Maluf NK, Silverman RH & Barton DJ (2008) A viral RNA competitively inhibits the antiviral endoribonuclease domain of RNase L. *RNA* **14**, 1026–1036.

3 Castelli JC, Hassel BA, Wood KA, Li XL, Amemiya K, Dalakas MC, Torrence PF & Youle RJ (1997) A study of the interferon antiviral mechanism: apoptosis activation by the 2-5A system. *J Exp Med* **186**, 967–972.

4 Díaz-Guerra M, Rivas C & Esteban M (1997) Activation of the IFN-inducible enzyme RNase L causes apoptosis of animal cells. *Virology* **236**, 354–363.

5 Zhou A, Paranjape J, Brown TL, Nie H, Naik S, Dong B, Chang A, Trapp B, Fairchild R, Colmenares C *et al.* (1997) Interferon action and apoptosis are defective in mice devoid of 2′,5′-oligoadenylate-dependent RNase. *EMBO J* **16**, 6355–6363.

6 Zhou A, Paranjape JM, Hassel BA, Nie H, Shah S, Galinski B & Silverman RH (1998) Impact of RNase L overexpression on viral and cellular growth and death. *J Interferon Cytokine Res* **18**, 953–961.

7 Castelli JC, Hassel BA, Maran A, Paranjape J, Hewitt JA, Li XL, Hsu YT, Silverman RH & Youle RJ (1998) The role of 2′-5′-oligoadenylate-activated ribonuclease L in apoptosis. *Cell Death Differ* **5**, 313–320.

8 Rusch L, Zhou A & Silverman RH (2000) Caspase-dependent apoptosis by 2′,5′-oligoadenylate activation of RNase L is enhanced by IFN-beta. *J Interferon Cytokine Res* **18**, 1091–1100.

9 Li G, Xiang Y, Sabapathy K & Silverman RH (2004) An apoptotic signaling pathway in the interferon antiviral response mediated by RNase L and c-Jun NH_2-terminal kinase. *J Biol Chem* **279**, 1123–1131.

10 Hattori H, Tanaka M, Fukushima M, Sasaki T & Matsuda A (1996) Nucleosides and nucleotides. 158. 1-(3-C-ethynyl-beta-D-ribo-pentofuranosyl)-cytosine, 1-(3-C-ethynyl-beta-D-ribo-pentofuranosyl)uracil, and their nucleobase analogues as new potential multifunctional antitumor nucleosides with a broad spectrum of activity. *J Med Chem* **30**, 5005–5011.

11 Takatori S, Tsutsumi S, Hidaka M, Kanda H, Matsuda A, Fukushima M & Wataya Y (1998) The characterization of cell death induced by 1-(3-*C*-ethynyl-beta-D-*ribo*-pentofuranosyl) cytosine (ECyd) in FM3A cells. *Nucleosides Nucleotides* **17**, 1309–1317.

12 Takatori S, Kanda H, Takenaka K, Wataya Y, Matsuda A, Fukushima M, Shimamoto Y, Tanaka M & Sasaki T (1999) Antitumor mechanisms and metabolism of the novel antitumor nucleoside analogues, 1-(3-*C*-ethynyl-beta-D-*ribo*-pentofuranosyl)cytosine and 1-(3-*C*-ethynyl-beta-D-*ribo*-pentofuranosyl)uracil. *Cancer Chemother Pharmacol* **44**, 97–104.

13 Naito T, Yokogawa T, Takatori S, Goda K, Hiramoto A, Sato A, Kitade Y, Sasaki T, Matsuda A, Fukushima M *et al.* (2009) Role of RNase L in apoptosis induced by 1-(3-*C*-ethynyl-beta-D-*ribo*-pentofuranosyl)cytosine. *Cancer Chemother Pharmacol* **63**, 837–850.
14 Brown MD & Sacks DB (2006) IQGAP1 in cellular signaling: bridging the GAP. *Trends Cell Biol* **16**, 242–249.
15 Johnson M, Sharma M & Henderson BR (2009) IQGAP1 regulation and roles in cancer. *Cell Signal* **21**, 1471–1478.
16 White CD, Brown MD & Sacks DB (2009) IQGAPs in cancer: a family of scaffold proteins underlying tumorigenesis. *FEBS Lett* **583**, 1817–1824.
17 Li Z, McNulty DE, Marler KJ, Lim L, Hall C, Annan RS & Sacks DB (2005) IQGAP1 promotes neurite outgrowth in a phosphorylation-dependent manner. *J Biol Chem* **280**, 13871–13878.
18 Yoshimura A, Nakanishi M, Yatome C & Kitade Y (2002) Comparative study on the biological properties of 2′,5′-oligoadenylate derivatives with purified human RNase L expressed in *E. coli*. *J Biochem* **132**, 643–648.
19 Lesiak K & Torrence PF (1986) Synthesis and biological activities of oligo(8-bromoadenylates) as analogues of 5′-O-triphosphoadenylyl(2′-5′)adenylyl(2′-5′)adenosine. *J Med Chem* **29**, 1015–1022.
20 Ueno Y, Naito T, Kawada K, Shibata A, Kim HS, Wataya Y & Kitade Y (2005) Synthesis of novel siRNAs having thymidine dimers consisting of a carbamate or a urea linkage at their 3′ overhang regions and their ability to suppress human RNase L protein expression. *Biochem Biophys Res Commun* **330**, 1168–1175.
21 Ueno Y, Kawada K, Naito T, Shibata A, Yoshikawa K, Kim HS, Wataya Y & Kitade Y (2008) Synthesis and silencing properties of siRNAs possessing lipophilic groups at their 3′-termini. *Bioorg Med Chem* **16**, 7698–7704.
22 Ausubel FM, Brent R, Kingston RE, Moore DD, Seidman JG, Smith JA & Struhl K (1999) *Current Protocols in Molecular Biology*, Vol. 2, *Immunoprecipitation*, Unit 10.16.1–10.16.29. John Wiley & Sons, Inc.
23 Sato A, Satake A, Hiramoto A, Wataya Y & Kim HS (2010) Protein expression profiles of necrosis and apoptosis induced by 5-fluoro-2′-deoxyuridine in mouse cancer cells. *J Proteome Res* **9**, 2329–2338.

Supporting information

The following supplementary material is available:
Fig. S1. Isolation of RNase L-binding proteins.
Fig. S2. Knockdown of IQGAP1 by RNA interference.

This supplementary material can be found in the online version of this article.

Please note: As a service to our authors and readers, this journal provides supporting information supplied by the authors. Such materials are peer-reviewed and may be re-organized for online delivery, but are not copy-edited or typeset. Technical support issues arising from supporting information (other than missing files) should be addressed to the authors.

research articles Journal of proteome research

Protein Expression Profiles of Necrosis and Apoptosis Induced by 5-Fluoro-2′-deoxyuridine in Mouse Cancer Cells

Akira Sato, Akito Satake, Akiko Hiramoto, Yusuke Wataya, and Hye-Sook Kim*

Faculty of Pharmaceutical Sciences, Okayama University, Tsushima, Okayama 700-8530, Japan

Received November 17, 2009

We have investigated the molecular mechanisms regulating the necrosis and apoptosis that occur on treatment of mouse mammary tumor FM3A cells with 5-fluoro-2′-deoxyuridine (FUdR), a potent anticancer agent, using the original clone F28-7 and its variant F28-7-A cells. Previously, we reported an interesting observation that FUdR induces a necrotic morphology in F28-7 but an apoptotic morphology in F28-7-A cells. We have now analyzed the protein expression profiles of these FUdR-induced necrosis and apoptosis. Thus, proteome analysis of these clones by two-dimensional gel electrophoresis and mass spectrometry showed that the cytoplasmic intermediate filament protein, cytokeratin-19, is expressed at a significantly higher level in F28-7 than in F28-7-A cells. This strong expression was detected both in untreated and FUdR-treated stages of F28-7 cells. We interpreted this phenomenon as suggesting that cytokeratin-19 possesses a function in leading the cell to apoptosis. We performed a knockdown of cytokeratin-19 expression in F28-7 cells by use of the small interfering RNA technique. Indeed, a lowering of the cytokeratin-19 expression down to the level in F28-7-A occurred, and the FUdR-induced death morphology of this knockdown F28-7 was apoptosis, instead of the necrosis usually observable in the FUdR-treated F28-7. It is known that the cytoskeletal protein cytokeratin-19 undergoes caspase-mediated degradation during apoptosis. Our present finding provides an interesting possibility that cytokeratin-19 may have a key role in regulating cell-death morphology.

Keywords: apoptosis • cell death • cytokeratin-19 • 5-fluoro-2′-deoxyuridine (FUdR) • intermediate filament • lamin B1 • necrosis • proteome analysis • siRNA

Introduction

Transcriptome and proteome analyses have been performed extensively to identify candidate genes and proteins involved in biological processes. A technique well suited for the analysis of protein compositions, modifications, and translocations is proteome analysis based on two-dimensional gel electrophoresis (2-DE) and mass spectrometry.[1] In cancer research, the subject of cell death is important for achieving therapeutic induction of cancer-cell-selective death. Among these two major forms of cell death, apoptosis and necrosis, apoptosis has received a proportionately greater degree of attention than has necrosis.[2,3] Proteome analysis has been used extensively to study apoptosis in cells, and more than 100 proteins have been identified as participants in the apoptosis.[4] However, this approach has been seldom applied for studies of necrosis.

We have investigated the molecular mechanisms regulating necrosis and apoptosis that occur on treatment of mouse mammary tumor FM3A cells with 5-fluoro-2′-deoxyuridine (FUdR), using the original clone F28-7 and its variant F28-7-A cells.[5,6] FUdR, a potent anticancer agent, exerts its effect by inhibiting thymidylate synthase, an essential machinery for DNA synthesis in cell proliferation (see ref 7 and references therein). Previously, we reported that the treatment can induce in F28-7 cells a breakdown of DNA into chromosome-sized fragments leading to necrosis, and that it can induce in F28-7-A more extensive DNA cleavage into oligonucleosome-sized fragments and subsequent development of apoptosis.[5] Through our recent studies on the gene expression profiles during the cell-death induced by FUdR, we proposed possible mechanisms associated with the necrosis and apoptosis.[6]

We have aimed at gaining more comprehensive insights into the cellular mechanisms activated during necrosis and apoptosis. The proteome of a cell is highly dependent on the conditions to which the cell is exposed and may respond in a quite complex manner. Current development of proteomics has now enabled us to analyze the protein expression profiles of necrosis induced by FUdR in F28-7 cells and those of apoptosis in F28-7-A cells. Here, we describe the patterns of differentially expressed proteins between these cells, as revealed by the proteome analysis. Also, phenotypic screening by use of small interfering RNAs (siRNAs) led to detection of a number of differentially expressed proteins in these cells. Using this approach, we identified two new regulators of the cell death: the nuclear inner membrane protein lamin B1[8] and the cytoplasmic intermediate filament-protein cytokeratin-19 (this report). A knockdown of cytokeratin-19 expression in F28-7 cells was performed by use of the siRNA technique, resulting in a decreased expression of cytokeratin-19 down to the level

* To whom correspondence should be addressed. Corresponding author: Dr. Hye-Sook Kim, Faculty of Pharmaceutical Sciences, Okayama University, Tsushima, Okayama 700-8530, Japan. Tel., +81-86-251-7975; Fax, +81-86-251-7974; E-mail, hskim@cc.okayama-u.ac.jp.

10.1021/pr9010537 © 2010 American Chemical Society

Published on Web 02/15/2010

in F28-7-A which is prone to apoptotic death. Remarkably, the FUdR-induced death morphology of this knocked-down F28-7 was apoptosis, clearly different from the necrosis that occurs in the FUdR-treated original F28-7.

Materials and Methods

Reagents, Antibodies, Cell, and Cell Culture. 5-Fluoro-2′-deoxyuridine (FUdR) was obtained from Sigma. FUdR was stored as 2 mM stocks in HPLC-grade water at −20 °C. 4′,6-Diamidino-2-phenylindole dihydrochloride (DAPI) was from Invitrogen. A set of four siRNAs against cytokeratin-19 mRNA was used: Mm_Krt1−19_1 FlexiTube siRNA, Catalog number SIO1085735; Mm_Krt1−19_2 FlexiTube siRNA, Catalog number SIO1085742; Mm_Krt1−19_3 FlexiTube siRNA, Catalog number SIO1085749; and Mm_Krt1−19_4 FlexiTube siRNA, Catalog number SIO1085756. AllStars Negative Control siRNA, Catalog number 1027280, was used as a nonsilencing siRNA. These siRNAs were obtained from Qiagen. The primary antibodies, rabbit polyclonal antihuman keratin-19 (K19) and rabbit polyclonal antikeratin-8 antibody, were from ANASPEC. Rabbit polyclonal anti-Annexin-A1 antibody and rabbit polyclonal antiglyceraldehyde-3-phosphate dehydrogenase (GAPDH) antibody were from Abcam and Trevigen, respectively. The secondary antibodies; antimouse IgG horseradish peroxidase-linked whole antibody and antirabbit IgG horseradish peroxidase-linked whole antibody were from GE Healthcare.

Original-type F28-7 clone and variant F28-7-A clone of mouse mammary tumor FM3A cells used in the study have been described previously.[5] The cells were cultured in ES medium (Nissui Pharmaceuticals), supplemented with 2% fetal bovine serum (Gibco) and 0.03% L-glutamine (Wako), in a humidified atmosphere with 5% CO_2 at 37 °C. Under these conditions, the doubling time of both F28-7 and F28-7-A cells was approximately 12 h.

F28-7 and F28-7-A cells (approximately 5×10^5 cells/mL) were treated with 1 μM FUdR. Cell viability was estimated with a hemocytometer by means of trypan blue-exclusion.

Two-Dimensional Gel Electrophoresis (2-DE). Cells were cultured, collected, and washed in ice-cold phosphate-buffered saline (PBS) and then lysed in 1.5 mL of Ready Prep Rehydration/Sample buffer (8 M urea, 2% CHAPS, 50 mM DTT, 0.001% bromophenol blue, and 0.2% w/v Bio-Lyte 3/10 ampholytes) prepared according to the manufacturer's instructions (Bio-Rad), with supplemental addition of Protease-Inhibitor Cocktail for Mammalian Cell (Sigma). The cells were sonicated on ice using Branson sonifier 250, then the lysate was left at room temperature for 30 min. The cell lysate was centrifuged at 10 000× *g* for 15 min at room temperature and the supernatant containing the solubilized proteins was used directly or stored at −80 °C prior to use. Protein concentrations were determined using the Lowry-method-oriented RCDC protein assay reagent (Bio-Rad). Protein samples from at least three independent experiments were collected for 2-DE analysis. The proteins were separated by large 2-DE (gel size 18 cm × 20 cm). Briefly, samples containing 200 μg of protein in 350 μL Rehydration/Sample buffer were loaded on the immobilized pH gradient (IPG) strips (ReadyStrips IPG Strips, 17 cm, pH range 3−10 nonlinear: Bio-Rad). Active rehydration and isoelectric focusing (IEF) were performed at 20 °C using PROTEAN IEF Cell (Bio-Rad). After active rehydration (50 V) for at least 12 h, IEF was performed in three steps, that is, conditioning (15 min at 250 V), voltage ramping (250−10,000 V in 2 h), and focusing (5 h at 10 000 V). The current was set at <50 μA per strip. Samples were subjected to reduction/alkylation prior to second dimension electrophoresis. Thus, the strips were incubated for 20 min in an equilibration buffer containing 2% (w/v) DTT, 6 M urea, 2% (w/v) SDS, 375 mM Tris, pH 8.8, and 20% (w/v) glycerol, then for 10 min in the same solution substituting DTT with 2.5% (w/v) iodoacetamide (Bio-Rad). Both of these steps were performed at room temperature. The strip was then sealed on top of the SDS-polyacrylamide gel using a 1% agarose solution. The run on the second dimension was carried out on an 12% polyacrylamide gel (Bio-Rad). Electrophoresis was performed at 20 °C for the first 30 min at 16 mA per gel, followed by 5 h at 24 mA per gel, on a PROTEAN II XL Cell system (Bio-Rad). Gels were fixed for 30 min in 7% acetic acid containing 10% ethanol and stained in the dark at room temperature for at least 16 h with 250 mL per gel of SYPRO Ruby stain (Bio-Rad). Gels were destained in 7% acetic acid containing 10% methanol for 1 h and scanned with the Molecular Imager FX (Bio-Rad).

Image Analysis. After scanning, the gel images were analyzed using PDQuest software, version 7.1.1 (Bio-Rad). Scanned gel images were processed to remove backgrounds and to automatically detect spots. For all spot intensity calculations, normalized values were used. Normalization of spot intensity was done so that the total sum of intensities in a gel would be equal to 1 000 000, and normalized spot intensities were expressed in ppm. The Student's *t*-test was performed, comparing protein expression in the SYPRO Ruby-stained 2D gels of F28-7 and F28-7-A cells in untreated or FUdR-treated stage ($n = 3$, $p < 0.05$).

Tryptic Digestion. Protein spots to be identified were excised from the 2-DE gels using an EXQuest Spot Cutter (Bio-Rad) and placed into a 96-well microtiter plate. The gels were washed twice with water, shrunk with acetonitrile, and dried in a SpeedVac. Then, samples were digested with 12.5 ng/μL porcine methylated trypsin (Promega) in 40 mM ammonium bicarbonate for at least 4 h at 37 °C.

MALDI-TOF MS, MALDI-TOF/TOF MS, and LC−MS/MS Analyses. The mass spectra were recorded by using Autoflex, Autoflex-III (Bruker Daltonics, Bremen, Germany), and HPLC-Chip-MS (Agilent Technologies, Santa Clara, CA). For MALDI-TOF MS and MALDI-TOF/TOF MS analyses, 2 μL of extracted peptides was spotted onto a Prespotted AnchorChip target-plate (Bruker Daltonics #227463) for MALDI-TOF analysis. MALDI MS measurements were performed in the mass range of 650−2600 Da on Autoflex and Autoflex-III mass spectrometers, set to reflectron mode, after calibration using a mixture of Anchor-spotted calibration standards (Bruker Daltonics). Mass spectra were determined as the sum of 200 laser shots. Also, the HPLC-Chip-IT-MS/MS experiments were performed on an Agilent 1100 LC/MSD-Trap-XCT series system. The ionization system was the Chip Cube using HPLC-Chip-MS. The chip was automatically loaded and positioned into the MS nanospray chamber. The chip contained a Zorbax 300SB-C_{18} (40 nL, 5 μm) enrichment column and a Zorbax 300SB-C_{18} (43 mm × 75 μm, 5 μm) analysis column. The sample loading into the enrichment column was performed at a flow rate set at 4 μL/min with a 0.1% HCOOH in H_2O. LC gradient (mobile phase-A: 0.1% HCOOH in H_2O; mobile phase-B: 0.1% HCOOH and 10% H_2O in CH_3CN) was delivered with the flow rate set at 300 nL/min. Tryptic peptides were eluted from the reversed-phase column into the mass spectrometer using a linear gradient elution of 4−85% phase-B over 40 min. The capillary

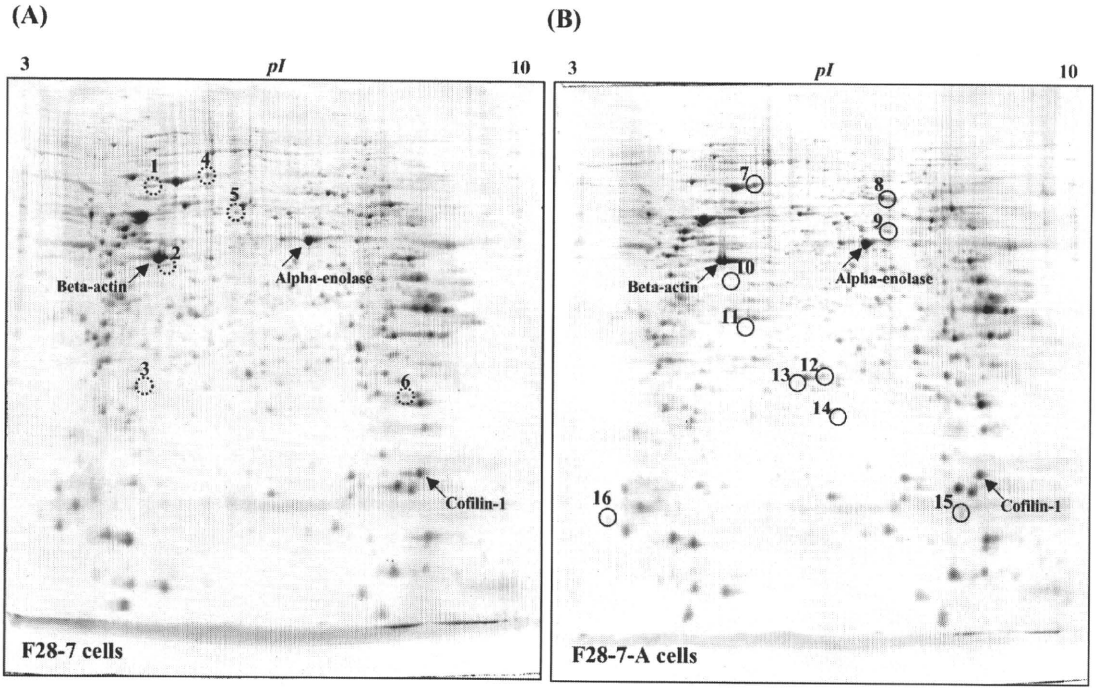

Figure 1. Sypro Ruby-stained 2D gels of F28-7 and F28-7-A cells in untreated stage. (A) Proteome 2D-map of F28-7 cells (two additional independent experiments gave essentially identical results). (B) Proteome 2D-map of F28-7-A cells (reproducibility confirmed; $n = 3$). Whole cell lysates were prepared from F28-7 and F28-7-A cells, and the individual lysates were focused on a pH 3–10 nonlinear range IPG strip and then separated on a 12.5% SDS-PAGE gel, stained, and visualized as described under "Experimental Procedures". The spots 1–6 displayed in the 2D-map of F28-7 cells (A) gave corresponding spots of lower intensities for F28-7-A (B). The spots 7–16 displayed in the 2D proteome map of F28-7-A cells (B) gave corresponding spots of lower intensities for F28-7 cells (A). Protein spots are identified by MALDI-TOF/MS, and nano LC–MS/MS.

voltage was set to 1850 V and the flow and the temperature of the drying gas were 4 L/min and 300 °C, respectively.

Database Searching. With MALDI-TOF/MS analysis, the proteins were identified by the peptide mass fingerprinting (PMF) and/or MS/MS ion search using MASCOT search engine (version 2.2.6; Matrix Science, London, UK). The Swiss-Prot database (release 57.13 of 19-Jan-2010; 514 212 sequences; 180 900 945 residues) was used for the searches. For PMF analysis, the peptide masses were exported to Biotools software version 3.2 (Autoflex, Bruker Daltonics) and used to perform a MASCOT search engine. Search parameters allowed a mass deviation of ±150 ppm, matching peptides containing one miscleavage, selection of species (*Mus musculus*), fixed modification of carbamidomethylated cysteines, and a variable modification of oxidized methionines. MASCOT protein scores greater than 48 were considered as significant ($p < 0.05$). In the MS/MS analysis, search parameters were set so that they allowed the peptide mass tolerance at ±150 ppm, and the fragment ion tolerance at ±0.5 Da. The allowance also included matching peptides containing one miscleavage, selection of species (*Mus musculus*), fixed modification of carbamidomethylated cysteines, and a variable modification of oxidized methionines. MASCOT protein scores (based on MS/MS spectra) of greater than 54 were considered statistically significant ($p < 0.05$). The individual MS/MS spectra with a statistically significant (confidence interval >95%) ion score were accepted. In the PMF and MS/MS ion search, the significance threshold for positive identification was determined by the Mascot Search program.

For HPLC-Chip/MS analysis, database searches were performed against the Swiss-Prot database (release 57.12 of 15-Dec-2009; 513 877 sequences; 180 750 753 residues) using a spectrum Mill MS proteomic workbench offered by Agilent (Software version Rev A. 03. 03. 084. SR4). The search parameters were set so that they allowed the peptide mass tolerance at ±2.5 Da, and the fragment ion tolerance at ±0.7 Da. The allowance also included matching peptides containing one miscleavage, selection of species (*Mus musculus*), fixed modification of carbamidomethylated cysteines, and a variable modification of methionine oxidation. Identification of proteins was validated when at least two peptide sequences matched with the database sequences, with concomitant occurrence of the peptide score greater than 11.

All MS and MS/MS spectra obtained were searched against the mouse protein database, which was collected from the Swiss-Prot (*Mus musculus*, 16 214 sequences) database.

The molecular masses and isoelectric points were calculated by employing the software Compute pI/MW (www.expasy.ch/tool/pi_tool.html).

Western Blot Analysis. Cells were washed in ice-cold PBS and then whole cell lysates were prepared using Laemmili sample buffer (Bio-Rad). Proteins (5×10^4 cells per lane) were subsequently fractionated under reducing conditions by 7.5% SDS-polyacrylamide gel electrophoresis and blotted onto a polyvinylidene difluoride membrane (Millipore). The membrane was then blocked against nonspecific binding by treatment for 1 h with 5% bovine serum albumin in Tris-buffered saline containing 0.1% Tween 20, and then immunoblotted overnight at 4 °C using the respective primary antibody. Next, the membrane was incubated for 1 h at room temperature with a horseradish peroxidase-conjugated antimouse IgG or antirabbit IgG secondary antibody, and the protein bands were visualized using an ECL plus Western blotting detection system (GE Healthcare). Protein expression

Table 1. Differential Protein-Spots from F28-7 and F28-7-A

spot no.	fold difference[a]	accession no.[b]	protein name	biological process (function)	theoretical p*I*	theoretical MW (Da)
			Spots stronger in F28-7 than in F28-7-A			
1	2.4	P14733	Lamin B1	Chromatin modificaton	5.11	66785.60
2[c]	3.3	P19001	Keratin, type I cytoskeletal 19 (Cytokeratin-19)	Cytoskeleton organization	5.28	44541.80
3	5.0	P10107	Annexin A1	Signal transduction	6.97	38734.30
4	2.0	P38647	Stress-70 protein, mitochondrial (GRP 75)	Protein folding	5.91	73528.33
5	2.0	P11679	Keratin, type II cytoskeletal 8	Cytoskeleton organization	5.70	54565.31
6	2.5	P19157	Glutathione S-transferase P1	Glutathione metabolism	7.69	23609.18
			Spots weaker in F28-7 than in F28-7-A			
7	0.2	P38647	Stress-70 protein, mitochondrial (GRP 75)	Protein folding	5.91	73528.33
8	0.6	P48678	Lamin-A/C	Chromatin modificaton	6.54	74237.57
		Q60864	Stress-induced phosphoprotein 1	Stress response	6.40	62582.11
		Q9CWJ9	Bifunctional purine biosynthesis protein PURH	Purine nucleotide biosynthesis	6.30	64217.38
9	0.4	Q9JLJ2	4-trimethylaminobutyraldehyde dehydrogenase (Aldehyde dehydrogenase 9A1)	Carnitine metabolism	6.63	53514.72
		P50431	Serine hydroxymethyltransferase, cytosolic	Glycine metabolism	6.47	52584.87
		Q8C1B7	Septin-11	Cell cycle	6.24	49694.64
10	0.6	Q9CQM9	Glutaredoxin-3	Redox homeostasis	5.42	37778.38
		Q8BK64	Activator of 90 kDa heat shock protein ATPase homologue 1 (AHA1)	Protein folding	5.41	38117.13
11	0.3	Q9QZH3	Peptidyl-prolyl cis−trans isomerase E	Protein folding	5.41	33448.85
12	0.6	O08807	Peroxiredoxin 4	Redox homeostasis	6.67	31052.52
13	0.5	Q60631	Growth factor receptor-bound protein 2	Signal transduction	5.89	25238.41
14	0.4	Q99LP6	GrpE protein homologue 1, mitochondrial	Protein folding	8.58	24307.02
		Q99LX0	Protein DJ-1	Protein folding	6.32	20021.31
15	0.3	P50446	Keratin, type II cytoskeletal 6A	Cytoskeletone organization	8.04	59335.12
16	0.4	Q8CGP5	Histone H2A type 1-F	Chromatin modificaton	11.05	14161.53

[a] Fold difference (F28-7/F28-7-A cells) > 1.5 or ≤ 0.6. [b] Swiss-prot primary accession number. [c] See graphic below. Bold-lettered peptide sequences indicate the identified peptides by MS/MS experiments in MALDI-TOF and/or nano-LC−MS/MS.

Spot No. 2

Keratin, type I cytoskeletal 19 (P19001)

MTSYSYR**QTS AMSSFGGTGG GSVRIGSGGV FR**APSIHGGS GGRGVSVSST R**FVTSSSGSY GGVRGGSFSG TLAVSDGLLS GNEKITMQNL NDRLASYLDK** VR**ALEQANGE LEVK**IRDWYQ KQGPGPSR**DY NHYFK**TIEDL R**DKILGATID NSKIVLQIDN ARLAADDFRT** KFETEHALRL SVEADINGLR **RVLDELTLAR** TDLEMQIESL KEELAYLKK**N HEEEITALRS** QVGGQVSVEV DSTPGVDLAK ILSEMR**SQYE IMAEKNRKDA EATYLARIEE LNTQVAVHSE QIQISKTEVT DLRRTLQGLE IELQSQLSMK AALEGTLAET EAR**YGVQLSQ IQSVISGFEA QLSDVRADIE RQNQEYKQLM DIK**SRLEQEI ATYRSLLEGQ EAHYNNLPTP KAI**

was quantified using VersaDoc imaging system (Bio-Rad). The following antibodies were used: anticytokeratin-19 antibody (1:200), anti-GAPDH antibody (1:10 000), antimouse IgG horseradish peroxidase-linked whole antibody (1:20 000), and antirabbit IgG horseradish peroxidase-linked whole antibody (1:20 000).

Transfection. Exponentially growing 2×10^5 cells were suspended in 75 μL siPORT electroporation buffer (Ambion) containing cytokeratin-19 siRNA cocktail or nonsilencing siRNA (final concentration 8×10^{-7} M) and introduced into 0.1 cm gap electroporation cuvette (Bio-Rad). The cytokeratin-19 siRNA cocktail was prepared by mixing Mm_Krt1−19_1, Mm_Krt1−19_2, Mm_Krt1−19_3, and Mm_Krt1−19_4 Flexi-Tube siRNAs. Cells were then electroporated using the Bio-Rad Gene Pulser Xcell at voltage 0.15 kV, pulse length 1000 μs, and number of pulse 1. After electroporation, cells were plated at 5×10^4 cells/mL in fresh ES medium in tissue culture flasks. Forty-eight hours after the electroporation, cells were used for further experiments.

Results

Protein Expression Analysis of Mouse Mammary Tumor FM3A Cells F28-7 and F28-7-A. Cell lysates were analyzed using 2-DE to detect changes in the proteome of F28-7 and F28-7-A cells. Figure 1A and B show typical two-dimensional gels of F28-7 and F28-7-A cell-lysates. Approximately 1800 protein spots per gel were detected within a pI range of 3−10 and a relative molecular mass range of 10−150 kDa. These data were reproducible in two additional independent experiments using newly cultured cells. With a 1.5-fold cutoff, that is, either >1.5 or <0.6, the analysis picked up 16 spots as having different intensities between F28-7 and F28-7-A. Spots 1−6 (Figure 1A) gave higher intensities in F28-7 than in F28-7-A; and Spots 7−16 (Figure 1B) gave lower intensities in F28-7 than in F28-7-A. Twenty-two proteins were identified in these 16 spots by MS analysis using MALDI-TOF/MS and nano LC−MS/MS. Of these 22 proteins, 6 were consistently higher and 16 were consistently lower in abundance in the F28-7 cells. Table 1 lists the names